3D holographic PTV measurements of micro-scale flows

Sang Joon Lee, Kyung Won Seo
Center for Biofluid and Biomimic Research, Department of Mechanical Engineering, Pohang University of Science and Technology, Pohang, 790-784, Republic of Korea
sjlee@postech.ac.kr http://bbrc.postech.ac.kr

Abstract: Holographic PTV (HPTV) is one of powerful means to get 3D (three-dimensional) velocity field information of flows. A micro-HPTV technique was developed and applied to measure 3D velocity fields of various micro-scale flows, including the flows in straight and curved micro-tubes having a circular cross-section and the 3D motion of red blood cells in a micro-tube. The inertial migration of neutrally buoyant micro-spheres suspended in a micro-tube was also investigated with varying Reynolds number and particle size. In addition, the motile characteristics of 3D motion of free-swimming chain-forming phytoplankton having different number of cells in various configurations were analyzed using the micro-HPTV technique. From time-varying 3D trajectories of swimming microorganisms, their swimming behaviors and swimming motion parameters were extracted successfully. Through these experiments, the micro-HPTV method was found to have strong potential in the accurate measurements of temporal variations of 3D velocity fields of various micro-scale flows and 3D motility of RBCs and microorganisms.

Key-Words: Digital holograpy, Holographic PTV, micro-scale flow, microorganism

1 Introduction

Holographic PIV/PTV techniques can measure 3D velocity fields in a 3D volume of complex flows [1,2]. By adopting digital holography, several cumbersome processes can be eliminated, such as chemical and physical handlings involved in hologram reconstruction and information acquisition [3, 4]. In digital holography, the hologram images of tracer particles in a flow are directly recorded using a digital image recording device, such as a charge-coupled device (CCD) or a complementary metal-oxide-semiconductor (CMOS) camera. The 3D flow information is subsequently obtained using numerical reconstruction and particle tracking procedures. However, the spatial resolution of the hologram is usually poor due to the finite size of pixels of commercial digital imaging devices. This limitation degrades the accuracy of measurement. To overcome this pixel size limitation, the in-line digital holographic microscopy (DHM) was developed by combining in-line digital holography and optical microscopy [5,6]. The basic concept of DHM is to magnify the hologram image by employing an optical lens system so that the microscopic fringes can be resolved at a high spatial resolution. The DHM technique has been applied to microscale flows for measuring 3C-3D velocity field information using the 3D PIV/PTV algorithm [7,8].

In the current study, the basic principle of DHM-PTV and its typical applications to microscale and biological flows are briefly reviewed [9–13].

2 Digital holographic PTV

Digital holography is an optical method for recording 3D volumetric field information on a digital hologram using a digital imaging device. The digital hologram is numerically reconstructed and then processed to extract 3D information. With the recent advances in in-line digital holography for analyzing fluid flows, obtaining time-resolved 3D field information by adopting a high-speed digital camera is now a possibility. The temporal evolution of 3D velocity field of a flow can be measured by applying the 3D particle tracking algorithm to the time series of holograms of particle fields. However, the digital imaging device adopted in holography suffers from limited spatial resolution. The spatial resolution of commercially accessible digital imaging sensors is approximately 100–200 lp/mm, which is lower than that of holographic film. As a result, the angular aperture of a digital hologram is smaller than that of film holograms. This angular aperture produces axial elongation of reconstructed particles, causing errors in determining the axial position of tracer particles. To overcome this technical problem, the DHM technique adopts the

ISBN: 978-1-61804-153-1

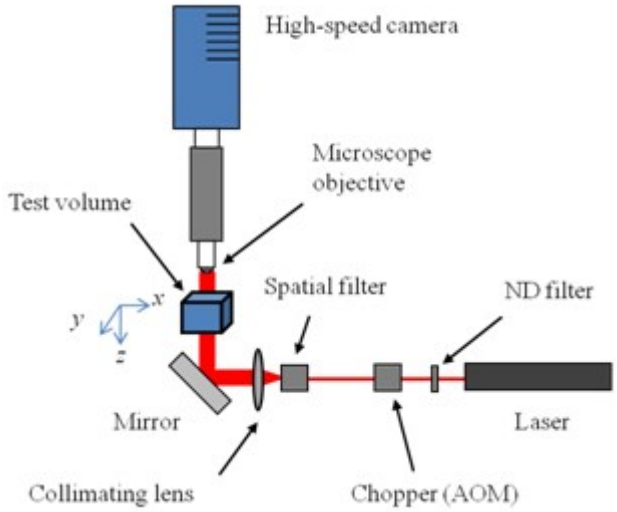

Figure 1. Experimental setup of digital in-line holographic microscope: AOM acts as a shutter to chop continuous laser beam into discrete pulses. The AOM and CCD camera are synchronized using a delay generator to capture images consecutively.

microscope objective lens in magnifying the hologram image. By using the DHM method, the pixel-size limitation of the image sensor array is relieved and the spatial resolution of digital holograms is significantly improved. In effect, the measurement accuracy along the light-propagation direction is further enhanced.

2.1 Hologram recording

Figure 1 shows a schematic diagram of DHM-PTV. A coherent laser beam is attenuated, spatially filtered, and collimated to produce a planar reference wave. The laser beam is then scattered by particles seeded in the flow and interfered with the unaffected reference wave, generating a hologram of tracer particles. The microscope objective lens magnifies it at the imaging plane of the digital camera, which records the hologram image. The DHM-PTV measurement can be expanded to 4D (space and time) by simply using a suitable high-speed digital camera. The recorded hologram images are then stored in the computer for digital image processing.

2.2 Digital hologram reconstruction

Prior to hologram reconstruction, the time-averaged background image is subtracted from the original raw holograms to eliminate the noises caused by optical components and misalignment. The background-subtracted hologram image is then numerically reconstructed to analyze the 3D positional information of the particles by employing the following Fresnel–Kirchhoff diffraction formula,

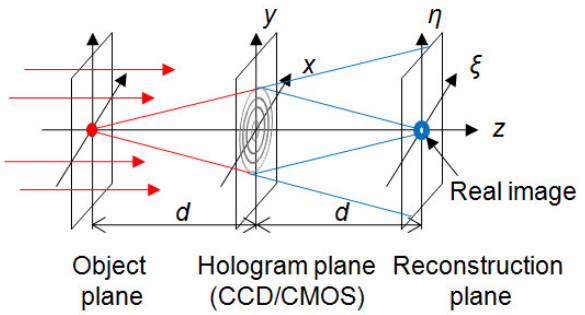

Figure 2 Coordinate system used for numerical reconstruction

which consists of the convolution between the hologram function *h(x,y)* and the diffraction kernel *g(x,y)* at each reconstruction plane:

$$\Gamma(\xi,\eta)=\frac{i}{\lambda}\int_{-\infty}^{\infty}\int_{-\infty}^{\infty}\mathrm{E}_R(x,y)h(x,y)\frac{\exp\left(-i\frac{2\pi}{\lambda}\rho\right)}{\rho}dxdy \quad (1)$$

$$\rho=\sqrt{d^2+(\xi-x)^2+(\eta-y)^2} \quad (2)$$

where ρ is the distance between a point in the hologram plane and a point in the reconstruction plane. The coordinate system of the numerical reconstruction is described in Fig. 2. Eq. 1 calculates the complex amplitude of the reconstructed wave field at a distance *d* from the hologram plane. To reconstruct the volume information of the object field, reconstruction should be performed through the whole volume with varying the reconstruction distance *d*.

The Fresnel–Kirchhoff integral of Eq. 1 can be interpreted as a convolution of the hologram function *h(x,y)* and of diffraction kernel *g(x,y)*:

$$\Gamma(\xi,\eta)=\{h(x,y)\otimes g(x,y)\}(\xi,\eta) \quad (3)$$

$$g(x,y)=\frac{i}{\lambda}\frac{\exp\left(-i\frac{2\pi}{\lambda}\sqrt{d^2+x^2+y^2}\right)}{\sqrt{d^2+x^2+y^2}} \quad (4)$$

From the convolution theorem, the integral can be efficiently calculated by using the 2D fast Fourier transforms (FFTs) as follows:

$$\Gamma(\xi,\eta)=\Im^{-1}\left[\Im\{h(x,y)\}\Im\{g(x,y)\}\right] \quad (5)$$

where $\Im$ and $\Im^{-1}$ denote the FFT and inverse-FFT, respectively. The intensity field of the reconstructed images can be obtained by taking the absolute $|\Gamma(\xi,\eta)|$.

2.3 Autofocus function for precise detection of particle position

After the reconstruction process, the 3D positional information of the particles is determined from the

ISBN: 978-1-61804-153-1

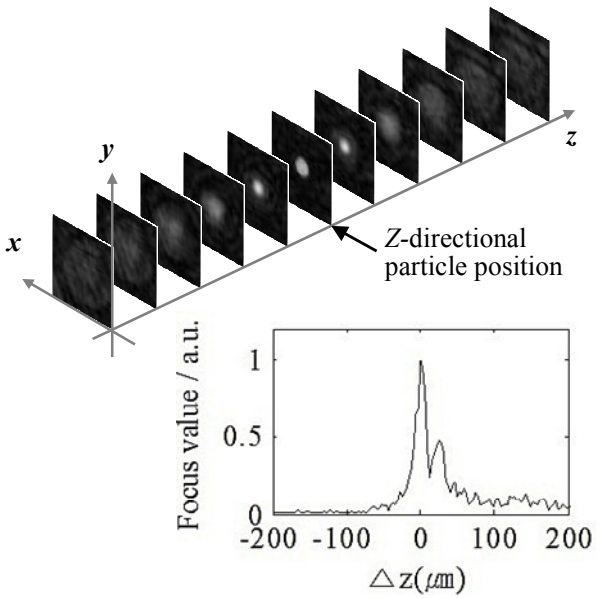

Figure 3. Reconstructed particle images and the corresponding focus value profile for a spherical particle of 7 μm in diameter.

reconstructed hologram. The in-plane (x, y) position of each particle is determined by searching the local intensity peak in the reconstructed image because the reconstructed particle has a higher intensity value than that of the background. After searching for the in-plane (x, y) position, the z-position of the particle is determined via an autofocus function, which quantifies the degree of image sharpness (i.e., focus value). Given that a reconstructed particle image has a maximum focus value when the reconstruction plane coincides with the actual particle position, the z-position of the particle is determined by searching the maximum focus value. The focus values can then be calculated using several autofocus functions defined as follows:

$$GRA(z) = \sum_{x,y} \left| \nabla I\left(x, y; z\right) \right| \qquad (6)$$

$$LAP\left(z\right) = \sum_{x,y} \left\{ \nabla^2 I\left(x, y; z\right) \right\}^2 \qquad (7)$$

$$VAR(z) = \frac{1}{N_x N_y} \sum_{x,y} \left\{ I\left(x, y; z\right) - \bar{I}\left(z\right) \right\}^2 \qquad (8)$$

where $I(x, y; z)$ represents the intensity distribution in a segment of the reconstructed image at a depth-wise plane z. The domain of x and y is restricted to a rectangular region enclosing a particle. $\bar{I}$ is the mean value of I, and N_x and N_y are the pixel dimensions of the segments. The above functions are used in quantifying the definition of an image as well as in searching the optimal focus plane [37, 38]. The performance of each focus function varies according to the shape and size of the tracer particles. Therefore, choosing the best autofocus function for the given experimental condition is recommended. Figure 3 shows typical reconstructed particle images and the corresponding focus value profile for a spherical particle 7 μm in diameter.

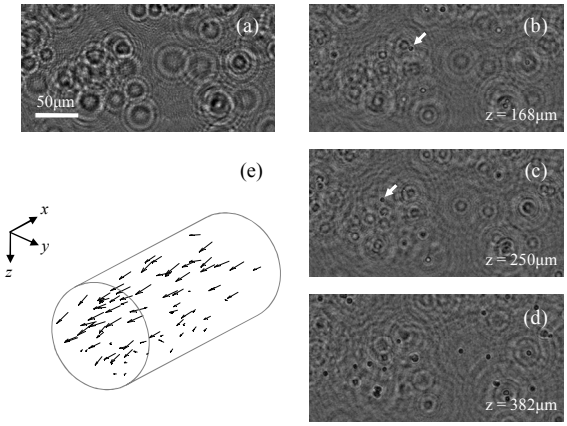

Figure 4. (a) Typical hologram of RBCs in a microtube flow; (b–d) reconstructed images at three selected depth planes wherein each focused RBC is marked by an arrow; and (e) 3D instantaneous velocity vectors of RBCs obtained from two consecutive holograms.

3 Applications to microscale flows

3.1 3D tracking of red blood cells in a microtube flow

Rently, the hemodynamic information of blood flows has been receiving much attention due to the rapid increase in the occurrence of circulatory vascular diseases. In the present study, 3D trajectories and velocity fields of RBCs flowing in a microtube are measured using the DHM-PTV technique. The experimental apparatus consists of a He-Ne laser, a spatial filter, a water-immersion objective lens (×20), and a high-speed digital camera. The RBC suspension diluted to a hematocrit of Hct = 0.05% is supplied to an FEP micro-tube (D =350 μm) immersed in water. Given that the refractive indices of the solution (plasma, n = 1.346), FEP tube (n = 1.338), and water (n = 1.333) are similar, the refractive distortion in the hologram image is prevented.

Figures 4 show a typical hologram image of RBCs and reconstructed images at three selected depth planes. In each reconstruction image, some RBCs are clearly observed in good focus. In the region near the bottom wall, the number of focused RBCs is increased because the density of RBC (ρ = 1.095) is slightly higher than that of the blood plasma (ρ=1.027). Figure 4e illustrates the instantaneous vectors of RBCs in the microtube

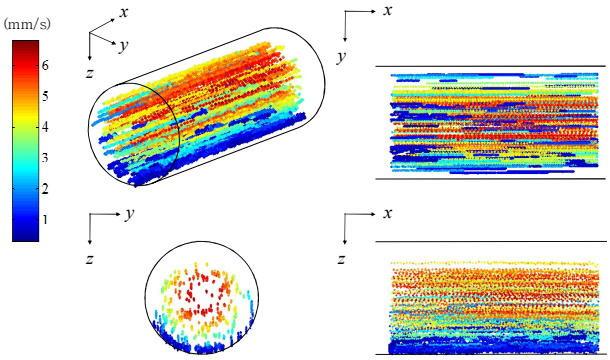

Figure 5. Trajectories of RBCs in a microtube flow. Color indicates the streamwise velocity of RBCs.

flow. The 4D (x, y, z, t) trajectories of tracked RBCs are shown in Figure 5. The trajectories of RBCs clearly indicate their linear movement. The velocity profile of RBCs is in good agreement with the Poiseuille velocity profile. Although some fluctuations are observed along the z-direction, the 3D motion of RBCs can be tracked with reasonable accuracy.

3.2 Inertial migration of microspheres

The inertial migration of particles in a Poiseuille flow can be utilized for practical applications, such as the passive separation or alignment of particles. The particles suspended in a Poiseuille flow tend to migrate across streamlines toward the equilibrium position at approximately 0.6 radii by the force balance between wall repulsion and inertial lift. In an axisymmetric Poiseuille pipe flow, the equilibrium position appears as a ring shape called Segré-Silberberg annulus [14]. On the contrary, there are four equilibrium positions near the center of each face in a square microchannel [15]. In the current study, the 3D positions of particles suspended in a microtube and in a square microchannel are measured using DHM-PTV.

The experimental setup consists of a continuous Nd:YAG laser, a water-immersion objective lens (×20), and a digital CMOS camera. The testing fluid is injected into the microtube (D = 350 μm, L = 300 mm) or the microchannel (H = 100 μm, L = 100 mm) using a syringe pump. Polystyrene microspheres (ρ_p = 1.05 g cm^{-3}) with mean diameters of a = 7–30 μm are mixed at a dilution of 0.05% w/v with water. The density of water is carefully matched with that of the particles by dissolving sodium chloride to attain neutral buoyancy. The Reynolds number $Re = U_m H/\nu$ is in the range Re = 4.7–120, where U_m is the maximum flow velocity, H is the hydraulic diameter, and ν is the kinematic viscosity. The ratios of the particle diameter to the hydraulic diameter are a/H = 0.04–0.16.

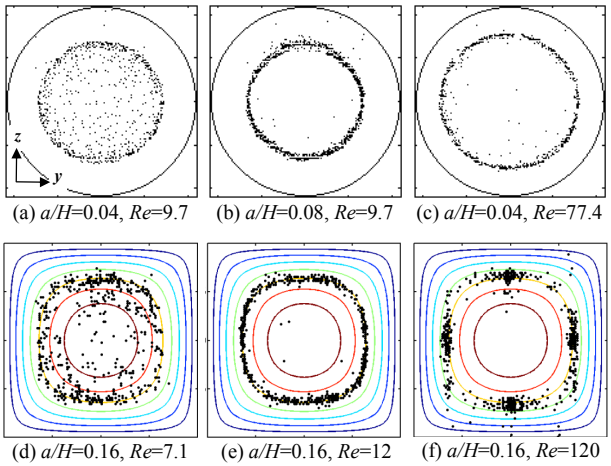

Figure 6. Spatial distribution of particles over a cross-sectional plane in a circular microtube and a rectangular microchannel.

From each of the hologram image, the 3D positional information of the particles are extracted and superimposed onto a cross-sectional (y, z) plane of the conduits to get the spatial distribution of the particles. Figure 6 shows the obtained spatial distributions of the particles in the two flows. As shown in Figures 6a–c, the tubular pinch effect of the particles is significant at a certain radial position, and the Segré-Silberberg annulus becomes obvious with increasing particle size and Re in microtube flow. Figures 6d–f illustrate the spatial distribution of particles in a square microchannel. As Re increases, the outward lateral migration in the central region becomes prevalent and a focused particle annulus is formed at a certain lateral position (Figure 6e). As Re is further increased, the particles begin to migrate cross-laterally toward the four equilibrium positions located near the center of each face (Figure 6f).

The Dean-coupled inertial migration of neutrally buoyant spherical particles that are suspended in a curved micro-scale pipe flow was experimentally investigated in the range of $6.4 \le Re \le 129$ and $1.69 \le De \le 34.1$ [16]. The three-dimensional positions of the particles were measured by using digital holographic microscopy. The diameter of the microtube was 350 μm, and the ratios of the tube diameter (D) to the particle diameter (d) were D/d = 12, 23, 35, and 50. The detailed structures of the Segré–Silberberg annulus as well as its deformation attributed to secondary flow were analyzed. Diverse agglomeration patterns of particles corresponding to the various flow conditions were observed

The secondary flow deforms the particle trajectories when the tubular-pinched particles pass through the curved section of the tube. The deformation of the

ISBN: 978-1-61804-153-1

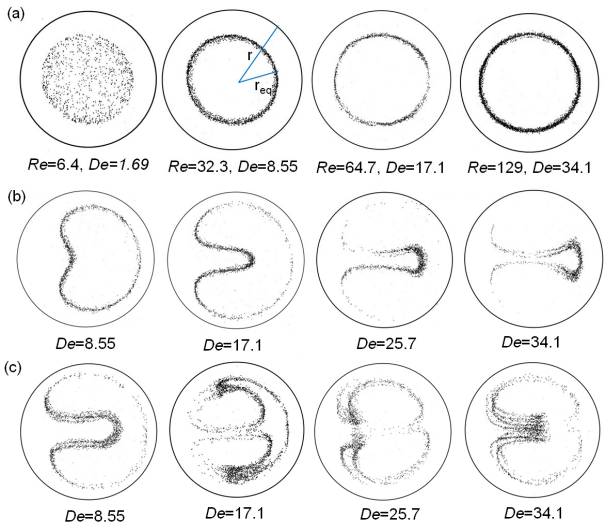

Figure 7. Cross-sectional views of particle distributions (D/d = 23) along a curved microtube (δ = 0.07) at (a) θ = 0°, (b) θ = 90°, and (c) θ = 180°.

circular particle annulus depends on the measurement location (θ) and on the value of *De*. The particle annuli, which are initially circular, were observed to change, and the unique agglomeration patterns of the particles appeared, as shown in Fig. 7. Figs. 7(b) and 7(c) show the cross-sectional position of the particles at two cross-sections with θ of 90° and 180°, respectively, and with varying values of *De*. Initially, the particles (d = 15 μm , D/d = 23) located near the inner bend (left side) start to migrate toward the outer bend (right side) along the horizontal midline of the tube cross-section at *De* = 8.55, as shown in Fig. 7(b). The particles that are positioned near the outer bend are swept along the top and bottom walls of the tube, and outward migration along the midline is further developed as *De* increases (Fig. 7). The cross-lateral migration of particles across the main flow is further developed at θ = 180° compared with those at θ = 90°, as shown in Fig. 7(c). The particle migration exhibits diverse distribution patterns according to *De* and θ.

3.3 3D motile characteristics of swimming microorganisms

Majority of the previous studies on motile characteristics of microorganisms have been performed using numerical simulation or 2D measurements. However, most microorganisms, such as flagellates, ciliates, and motile germ cells, inherently exhibit 3D swimming features. Therefore, to understand the motile behaviors of microorganisms in detail, accurate measurement of their 3D motions is strongly recommended. Recently, the digital holographic PTV technique has

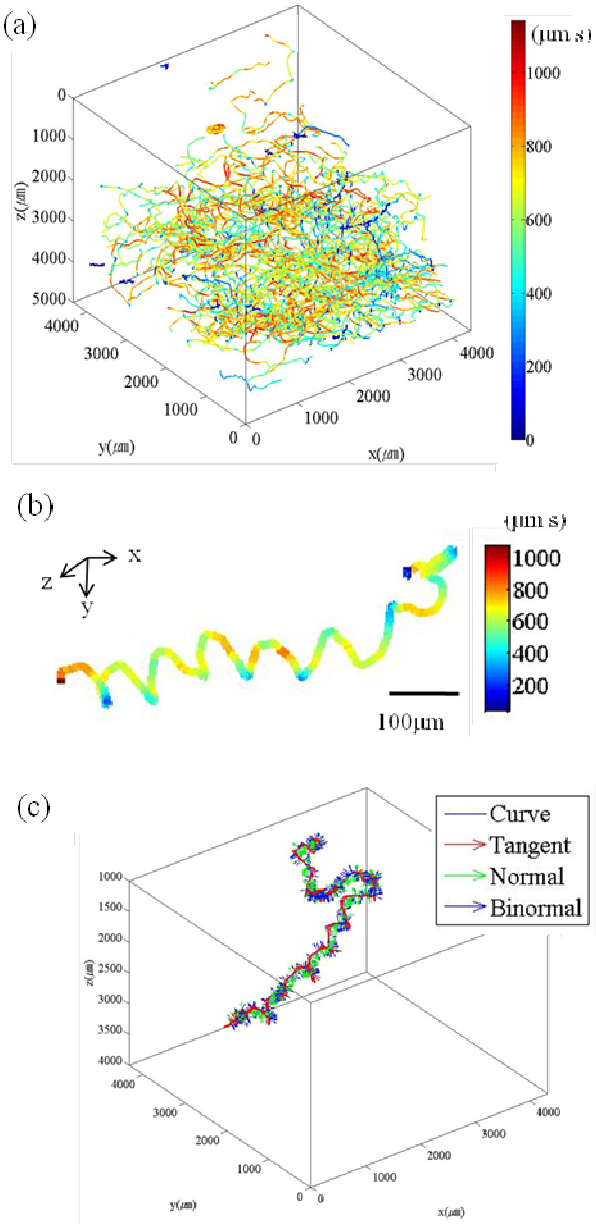

Figure 8. (a) Three-dimensional trajectories of free-swimming *C. Polykrikoides* with color-coded speed. (b) representative helical swimming trajectory of a 4-cell *C. polykrikoides* chain. (c) orientation variation of a swimming microorganism.

been employed in observing the 3D motion of microorganisms and in measuring the velocity fields induced by them.

In the present study, the 3D free-swimming motion of *C. polykrikoides*, a phytoplankton species that causes red tide, is measured using the DHM-PTV technique with a high depth-directional accuracy [13]. *C. polykrikoides* usually forms chains in the exponential and stationary growth phases. The chain-forming cells consist of 2, 4, 8, and, occasionally, 16 cells. A single *C. polykrikoides* cell has an ellipsoidal shape, with a length of 30–40 μm

ISBN: 978-1-61804-153-1

and a width of 25–30 μm. The sample chamber is made of BK7 glass windows with dimensions of $10\times10\times5$ mm^3. The size of the chamber is large enough for the cells to swim freely. A collimated He-Ne laser beam is used to illuminate the cells in the sample chamber. To magnify the hologram images, an objective lens (×4) is attached in front of the high-speed CMOS camera. The field of view is $4.3\times4.3\times5$ mm^3 with a spatial resolution of approximately 4.2 μm in the lateral direction.

Figure 8 shows the 3D swimming trajectories of several hundred *C. polykrikoides* cells with color-coded speed. Aside from the swimming trajectories and moving speed, the swimming attitude, orientations, and helices can be extracted as shown in Figure 8.

4 Conclusion

Due to advances in optics, laser, computer, and digital image processing techniques, digital holography becomes an essential tool for 3D measurements. In addition, the DHM-PTV technique is an ideal tool for measuring 3C-3D velocity field information of a microscale flow with a fairly good spatial resolution. Moreover, DHM-PTV system is composed of similar optical components as the conventional micro-PIV system. The advances in the DHM-PTV technique enable the measurement of various microscale flows in which 3D flow analysis is indispensible, such as transport of biological fluids in microvascular vessels and 3D flows in various microfluidic devices. DHM-PTV would play an important role in revealing the unknown basic physics of various microscale flow phenomena.

References:

[1] H. Meng, F. Hussain, In-line recording and off-axis viewing technique for holographic particle velocimetry, Appl. Opt. 34 (1995) 1827–1840.

[2] J. Sheng, E. Malkiel, J. Katz, Single beam two-views holographic particle image velocimetry, Appl. Opt. 42 (2003) 235–250.

[3] U. Schnars and W. Jüptner, Direct recording of holograms by a CCD target and numerical reconstruction, Appl. Opt. 33 (1994) 179–181.

[4] H. Meng, G. Pan, Y. Pu, S.H. Woodward, Holographic particle image velocimetry: from film to digital recording, Meas. Sci. Technol. 15 (2004) 673–685.

[5] W. Xu, M. H. Jericho, I. A. Meinertzhagen, H. J. Kreuzer, Digital in-line holography of microscopheres, Appl. Opt. 41 (2002) 5367–5375.

[6] S. Satake, T. Kunugi, K. Sato, T. Ito, J. Taniguchi, Three-dimensional flow tracking in a micro channel with high time resolution using micro digital-holographic particle-tracking velocimetry, Opt. Rev. 12 (2005) 442–444.

[7] J. Sheng, E. Malkiel, J. Katz, J. Adolf, R. Belas, A. R. Place, Digital holographic microscopy reveals prey-induced changes in swimming behavior of predatory dinoflagellates, Proc. Natl. Acad. Sci. USA, 104 (2008) 17512–17517.

[8] J. Sheng, E. Malkiel, J. Katz, Using digital holographic microscopy for simultaneous measurements of 3D near wall velocity and wall shear stress in a turbulent boundary layer, Exp. Fluids 45 (2008) 1023–1035.

[9] S. Kim, S.J. Lee, Measurement of Dean flow in a curved micro-tube using micro digital holographic particle tracking velocimetry, Exp. Fluids, 46 (2009) 255–264.

[10] Y.S. Choi, S.J. Lee, Three-dimensional volumetric measurement of red blood cell motion using digital holographic microscopy, Appl. Opt. 48 (2009) 2983–2990.

[11] Y.S. Choi, S.J. Lee, Holographic analysis of three-dimensional inertial migration of spherical particles in micro-scale pipe flow, Microfluid. Nanofluid. 9 (2010) 819–829.

[12] Y.S. Choi, K.W. Seo, S.J. Lee, Lateral and cross-lateral focusing of spherical particles in a square microchannel, Lab Chip, 11 (2011) 460–465.

[13] M.H. Sohn, K.W. Seo, Y.S. Choi, S.J. Lee, Y.S. Kang, Y.S. Kang, Determination of the swimming trajectory and speed of chain-forming dinoflagellate cochlodinium polykrikoides with digital holographic particle tracking velocimetry, Mar. Biol. 158 (2011) 561–570.

[14] G. Segré, A. Silberberg, Radial particle displacements in Poiseuille flow of suspensions, Nature, 189 (1961) 209–210.

[15] D. Di Carlo, J.F. Edd, K.J. Humphry, H.A. Stone, M. Toner, Particle segregation and dynamics in confined flows, Phys. Rev. Lett. 102 (2009) 094503

[16] K. W. Seo, Y. S. Choi, S. J. Lee, Dean-coupled inertial migration and transient focusing of particles in a curved microscale pipe flow, Exp. Fluids, (2012) published online